Heterologous Overexpression and Purification of Cytochrome *c*′ from *Rhodobacter capsulatus* and a Mutant (K42E) in the Dimerization Region. Mutation Does Not Alter Oligomerization but Impacts the Heme Iron Spin State and Nitric Oxide Binding Properties†

Wilhelmina M. Huston,‡ Colin R. Andrew,§ Amy E. Servid,§ Alison L. McKay,§ Andrew P. Leech,‡ Clive S. Butler,|| and James W. B. Moir*,‡

Department of Biology (Area 10), University of York, Heslington, York, YO10 5YW, United Kingdom, Institute for Cell and Molecular Biosciences, University of Newcastle, Newcastle upon Tyne, NE2 4HH, United Kingdom, and Department of Chemistry and Biochemistry, Eastern Oregon University, La Grande, Oregon 97850

Received December 21, 2005; Revised Manuscript Received February 13, 2006

ABSTRACT: *Rhodobacter capsulatus* cytochrome *c*′ (RCCP) has been overexpressed in *Escherichia coli*, and its spectroscopic and ligand-binding properties have been investigated. It is concluded that the heterologously expressed protein is assembled correctly, as judged by UV−vis absorption, EPR, and resonance Raman (RR) spectroscopy of the unligated protein as well as forms in which the heme is ligated by CO or NO. To probe the oligomerization state of RCCP and its potential influence on heme reactivity, we have compared the properties of wild-type RCCP with a mutant (K42E) that lacks a salt bridge at the subunit interface. Analytical ultracentrifugation indicates that wild-type and K42E proteins are both monomeric in solution, contrary to the homodimeric structure of the crystalline state. Surprisingly, the K42E mutation produces a number of changes at the heme center (nearly 20 Å distant), including perturbation of the ferric spin-state equilibrium and a change in the ferrous heme−nitrosyl complex from a six-coordinate/five-coordinate mixture to a predominantly five-coordinate heme−NO species. RR spectra indicate that ferrous K42E and wild-type RCCP both have relatively high Fe−His stretching frequencies, suggesting that the more favored five-coordinate heme−nitrosyl formation in K42E is not caused by a weaker Fe^{2+}−His bond. Nevertheless, the altered reactivity of ferrous K42E with NO, together with its modified ferric spin state, shows that structural changes originating at the dimer interface can affect the properties of the heme center, raising the exciting possibility that intermolecular encounters at the protein surface might modulate the reactivity of cytochrome *c*′ in vivo.

Cytochromes *c*′ are found in the periplasm of a metabolically diverse range of proteobacteria, including denitrifying, photosynthetic, sulfur oxidizing, and methylotrophic bacteria. They are characterized by relatively low redox potentials (∼10−150 mV) and have been extensively investigated spectroscopically due to their unusual magnetic properties. The heme iron has been shown to have a vacant sixth coordination site that is surrounded by what has been described as a hydrophobic cage (*1*). This cage favors the binding of small uncharged molecules such as NO and CO to the heme iron. Given the presence of cytochrome *c*′ within a diverse range of proteobacteria, the physiological role of cytochrome *c*′ is a key component of many investigations. It is widely postulated in the literature that the ability to bind NO is likely to be indicative of the physiological function of these proteins (*2*−*5*). Cross et al. showed that *Rhodobacter capsulatus* mutants deficient in *cycP*, (the gene encoding cytochrome *c*′) are more sensitive to NO than is a wild-type strain and showed a diminished ability to remove NO from solution (*5*, *6*). Similarly, investigations using a genetic mutant in *cycP* in *Neisseria meningitidis* demonstrated an increased sensitivity to NO in comparison to wild-type strain (*7*).

All reported crystal structures of cytochromes *c*′ (with the exception of *Rhodospirillum palustris* cytochrome *c*′) show the protein to be a homodimer (*8*−*14*). Each monomer consists of a four α-helix bundle with the covalently bound C-terminal heme located in the center of the helix bundle. Structural investigations have shown that the dimer interface varies between the proteins. Tahirov and co-workers have defined two different structural categories of the cytochrome *c*′, class 1 and class 2, on the basis of the dimer interface and the channel between helix B and C, which allows variable access to the vacant distal heme coordination site (*13*). According to this classification, the class 1 cytochromes *c*′, including that isolated from *R. capsulatus* (RCCP),[1] have less bulky residues along this channel allowing more accessibility to the heme. The intersubunit interactions are

† J.W.B.M. was supported by Grant No. 87/C19243 from the Biotechnology and Biological Sciences Research Council, UK. C.R.A. acknowledges support from the National Science Foundation (Grant MCB-0417152). CSB acknowledges OneNortheast for funding the EPR spectroscopy facility.

* To whom correspondence should be addressed. Telephone: +44 01904 328677. Fax: +44 01904 328828. E-mail: jm46@york.ac.uk. Address correspondence relating to EPR spectroscopy to C.S.B. E-mail: c.s.butler@ncl.ac.uk.

‡ University of York.

|| University of Newcastle.

§ Eastern Oregon University.

10.1021/bi052605j CCC: $33.50
Published on Web 03/21/2006

mainly hydrophobic in the dimers of *Chromatium vinosum* cytochrome *c*′ (CVCP) and *Rh. molischanarium* cytochrome *c*′ (RMCP) (*10*, *11*) whereas the *Rh. rubrum* cytochrome *c*′ (RRCP) dimers are formed by electrostatic interactions (*12*). The crystal structure of RCCP M110 shows that the dimer formation in this cytochrome *c*′ is quite unique as the interfaces consist of both hydrophobic and electrostatic interactions (*13*). Part of this interface is formed by a salt bridge between Lys42 and Glu39 from the neighboring subunits.

Although the vast majority of cytochromes *c*′ are dimeric in the crystalline state, there is evidence to suggest that cytochromes *c*′ might adopt different oligomerization states under certain conditions. For example, RCCP and *R. sphaeroides* cytochrome *c*′ are reported to exist in solution as an equilibrium of monomer and dimers (*15*). There have also been observations that subtle changes in sequence between different *R. capsulatus* strains can influence the dimer or monomeric structures in solution. Thus, RCCP isolated from M110 and related strains are usually found as predominantly a dimer in solutions unlike MT1131 and related strains in which RCCP isolates predominantly as a monomer in solution (*3*, *13*, *15*−*17*, *19*). RCCP from strain MT1131 forms a crystallographic dimer, but this requires the inclusion of zinc in the crystallization buffer. Some evidence exists that heme reactivity in cytochromes *c*′ may be linked to their oligomerization state. In particular, studies on CVCP have indicated that CO binding to the distal heme face disrupts the distal Tyr16 residue, which in turn causes tertiary changes at the subunit interface resulting in dimer dissociation (*8*, *21*, *23*). On the other hand, previous studies on RCCP have indicated that CO binding does not induce subunit dissociation (*9*).

Electron paramagnetic resonance (EPR) and other magnetic spectroscopies have shown that ferric cytochromes *c*′ exhibit an unusual spin-state equilibrium between a quantum-mechanically admixed high-spin/intermediate-spin (QS) state ($S = 5/2, 3/2$), and a pure high-spin (HS) species ($S = 5/2$) (*18*). These unusual spin properties are pH dependent, with the proportion of HS state increasing with pH. It has been proposed that the pH-dependent spin state is associated with a change in ionization state of the proximal His ligand (*19*, *21*). Ferric cytochromes *c*′ are known to react with NO to form six-coordinate ferric heme−nitrosyl complexes that are susceptible to reductive nitrosylation at high pH.

In the ferrous state, cytochromes *c*′ can bind CO and NO. The binding of CO yields a six-coordinate complex with the CO bound in a hydrophobic pocket on the distal side of the heme. NO binding is more intricate. Ferrous heme−nitrosyl complexes of cytochromes *c*′ can exist as mixtures of both six-coordinate and five-coordinate complexes, with the exact ratio dependent on the particular protein involved. In cytochrome *c*′ from *Alcaligenes xylosoxidans* (AXCP), NO binds to ferrous heme to form a heme−nitrosyl end-product that is mostly five-coordinate. Moreover, NO binds on the proximal side of the heme, displacing the His residue that ligates the heme iron in the absence of ligand (*20*). Yoshimura and colleagues suggest that the ratio of five- to six-coordinate NO bound complex can be correlated with the ratio of high to intermediate spin state of the ferric cytochrome *c*′ in the absence of ligand (*21*). We have recently argued that the heme−nitrosyl coordination number may be affected by the degree of steric hindrance to ligand binding in the distal pocket (*22*).

To unravel the factors influencing NO binding (and turnover) by the cytochromes *c*′, it is necessary to have an expression system so that purified proteins can be obtained and the influence of particular amino acids can be probed by mutagenesis. Here we report the first heterologous expression system for RCCP in *Escherichia coli*. We also describe the preparation and characterization of the K42E mutant in which an ionic interaction at the dimer interface has been abolished. Interestingly, our results reveal that the mutation does not alter oligomerization but instead impacts the heme iron spin state and nitric oxide binding properties.

EXPERIMENTAL PROCEDURES

Bacterial Strains and Culturing. E. coli DH5α was used as a general cloning vehicle. Protein expression was performed using *E. coli* BL21 λDE3 (Novagen, USA). *E. coli* were routinely cultured at 37 °C in LB medium or on LB plates containing 1.5% agar. Broth cultures where shaken at 190 rpm. Antibiotics ampicillin (50 μg/mL) and chloramphenicol (25 μg/mL) were used. *R. capsulatus* PAS100 was grown photosynthetically in RCV medium.

Generation of Plasmid Constructs. The *cycP* gene was amplified from the genome of *R. capsulatus* PAS100 (the cytochrome *c*′ gene product from this strain is identical to that from *R. capsulatus* strain MT1131) by PCR using the primers 5′-gggccatggctgataccaaagaagttcttg-3′ and 5′-tcagtcttcttcgcgatagtcg-3′. The restriction enzyme site for *Nco*I was incorporated into the primer design of the forward primer to enable directional cloning into the vector pET22b (Novagen, USA). The PCR product was amplified by PCR using *Pfu* polymerase (Promega, UK) with an annealing temperature at 61 °C and a 1 min 15 s extension time. The PCR product was initially cloned into pCRBlunt II (Invitrogen, USA) using a topoisomerase reaction according to the manufacturer's instructions prior to subcloning into the vector pET22b using the restriction enzymes NcoI and NotI to generate the vector pET22bRCCP. The product contains the coding region for the mature *R. capsulatus* cytochrome *c*′ cloned in frame with the sequence encoding the periplasmic leader sequence from *E. coli* gene *pelB*.

The site-directed mutant K42E was constructed by PCR. The primers used in this reaction were K42Efwd 5′-aaggtcgaagcggcc(g)agcttgaaaagatcctggcg-3′ and K42Erev 5′-cgcggcttcggcatcaaaggccttggccacgcc-3′. The incorporated mutation is indicated in parentheses where the sequence for the wild-type *cycP* gene contains a lysine (aag) this was changed to a glutamic acid (gag). PCRs were conducted using a 50 μL reaction mix containing a number of modifications to the recommended reaction conditions: 10−50 ng of the pET22bRCCP construct as described above, 150 pmol of

[1] Abbreviations: QS, quantum-mechanically admixed high-spin/intermediate-spin; HS, high spin; CVCP, *Chromatium vinosum* cytochrome *c*′; RMCP, *Rhodospirillum molischanarium* cytochrome *c*′; RRCP, *Rhodospirillum rubrum* cytochrome *c*′; RCCP, *Rhodobacter capsulatus* cytochrome *c*′; AXCP, *Alcaligenes xylosoxidans* cytochrome *c*′; ht-RCCP, wild-type *R. capsulatus* cytochrome *c*′ heterologously overexpressed in *Escherichia coli*; RCCP K42E, heterologously expressed *R. capsulatus* cytochrome *c*′ with site-directed mutagenesis of Lys42 to Glu; RR, resonance Raman; EPR, electron paramagnetic resonance.

each primer, 0.2 mM dNTPs, buffer (as provided by the manufacturer), additional 2.5 mM $MgCl_2$, *Pfu* polymerase (Promega, UK), 0.5 μL of 15% DMSO, and sterilized MilliQ water. The reactions were conducted with an annealing temperature of 68 °C, an extension time of 14 min 30 s for a total of 16 cycles. The PCR reactions were then digested overnight using the restriction enzyme DpnI at 37 °C, which was subsequently heat inactivated at 65 °C prior to the addition of ligase and 1 mM ATP and incubation for 5−24 h at 4 °C.

Overexpression and Purification Procedures for ht-RCCP and RCCP K42E. BL21 λDE3 pet22bRCCP pST2 was cultured aerobically in LB broth (15% flask volume, shaking at 190 rpm) until an O.D. at 600 nm of approximately 0.8 was reached. [pST2 is a plasmid containing the *ccm* genes from *E. coli* and conferring resistance to chloramphenicol (*24*)]. Coexpression of the *ccm* genes is necessary for assembly of *c*-type cytochromes in the *E. coli* periplasm under aerobic conditions. Cultures were induced with 1 mM IPTG, and growth continued for a further 3 h before cells were harvested by centrifugation at 4000*g* for 10 min at 4 °C. Cells were resuspended in 50 mM Tris pH 8.0, and sonicated for a total of 2 min using a Misonix 3000 sonicator, and the soluble material containing the expressed cytochrome was separated from particulate material by centrifugation at 4000*g* for 10 min. Total soluble extract (wild-type heterologously expressed RCCP (ht-RCCP) purity index (A_{400}/A_{280}): 0.041, RCCP K42E purity index: 0.046) from *E. coli* overexpression strains was initially loaded onto an anion exchange column using DEAE-CL6B packed into a column with a 60 mL bed volume. The cytochrome *c*′ eluted at approximately 300 mM NaCl when chromatography was conducted over a gradient of 0−500 mM NaCl in 50 mM Tris pH 8.0. The ht-RCCP eluted with a purity index of 0.192 and RCCP K42E with a purity index of 0.095. The fractions containing the cytochrome *c*′ were then concentrated by ammonium sulfate precipitation (0−90% saturation), and the resulting pellet was resuspended in a small volume of 10 mM potassium phosphate pH 7.0. The samples were then further purified by size exclusion chromatography utilized sephacryl S-200 (S-100) packed into a column with a 120 mL bed volume column. The ht-RCCP and RCCP K42E samples had purity indices of 0.59 and 0.60, respectively. The final step in the purification of the proteins was conducted via hydroxyapatite (Type I) chromatography where fractions containing the cytochrome *c*′ from gel filtration were pooled and loaded onto a 25 mL bed volume column containing Type I hydroxyapatite (Sigma-Aldrich, UK). Proteins were eluted over a gradient of 10−200 mM potassium phosphate pH 7.0. The ht-RCCP and RCCP K42E eluted at approximately 100 mM potassium phosphate with a purity index of 1.5 for ht-RCCP and 1.43 for RCCP K42E. Yields of approximately 1 mg of pure protein were obtained from 5 L cultures of *E. coli* overexpression strains. Protein purity was monitored by Coomassie and heme-stained gels (*25*, *26*).

Purification of Native RCCP from Rhodobacter capsulatus. The native RCCP was purified from cultures of *R. capsulatus* PAS100 (pRKMC401) grown photosynthetically using the procedure previously described (*6*).

Spectroscopic Methods. Electronic absorption spectra in the UV−vis range were obtained at room temperature in a Jasco 550 spectrophotometer. Samples contained in stoppered cuvettes were purged with nitrogen gas prior to saturation with NO or CO gas for measurement of ligand binding spectra. Electron paramagnetic resonance (EPR) spectra were measured using a Bruker EMX spectrometer (X-band 9.38 GHz) equipped with an ER4112HV liquid helium flow cryostat system. Ferricytochrome *c*′ spectra were recorded at 10 K, 4.0 G modulation amplitude, and 2.0 mW power. Secondary structure was monitored using far-UV circular dichroism (CD) in a Jasco J810. Resonance Raman (RR) spectra, from samples typically containing ∼100 μM in heme, were recorded on a custom McPherson 2061/207 spectrograph (set to 0.67 m) equipped with a Princeton Instruments liquid N_2-cooled (LN-1100PB) CCD detector and Kaiser supernotch filters. Heme−nitrosyl complexes were prepared using nitric oxide gas bubbled through 0.1 M KOH solution to remove higher oxides of nitrogen. Excitation wavelengths were provided by the 413.1-nm line of a Kr ion laser (Innova) or the 441.6-nm line of a He−Cd laser (Liconix 4240NB). RR spectra were obtained in a 90°-scattering geometry from samples at room temperature contained in glass capillaries. Photodissociation was minimized by the use of a reciprocating translation stage. Frequencies were calibrated relative to indene and CCl_4 and are accurate to ± 1 cm^{-1}. Optical absorption spectra of samples in their RR cells were checked before and after laser illumination using a modified Cary 50 spectrophotometer.

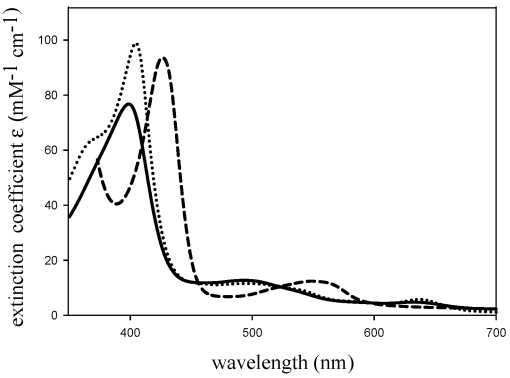

FIGURE 1: UV−vis absorption spectra of heterologously expressed RCCP spectra at pH 6.0 (solid line) and pH 10.5 (dotted line). The dithionite-reduced form of the protein at pH 7.0 is also depicted (dashed line). The Soret peak shifts from 399 to 404 nm on increasing pH. Other peaks for the ferric protein are at 500 and 635 nm. Ferrous peaks are centered at 430 and 550 nm.

Analytical Ultracentrifugation. Analytical ultracentrifugation (AUC) was conducted at room temperature in a Beckman Optima XL/I analytical ultracentrifuge. Protein was monitored using absorption at 495, 400, and 630 nm. Experiments were conducted in triplicate at 20 °C.

Pyridine Hemochrome. The pyridine hemochrome assay was used to determine total heme content of samples as previously described (*27*).

RESULTS

Spectroscopic Evidence that Recombinant RCCP Is Identical to Native RCCP. Solutions of heterologously expressed wild-type (ht-RCCP) display electronic absorption spectra (Figure 1) that are similar to those previously reported for native RCCP (*18*). At pH 6, ferric ht-RCCP has absorption maxima at 399, 500, and 635 nm. As the pH is increased to pH 10.5, the 399-nm peak shifts to 404 nm and increases in

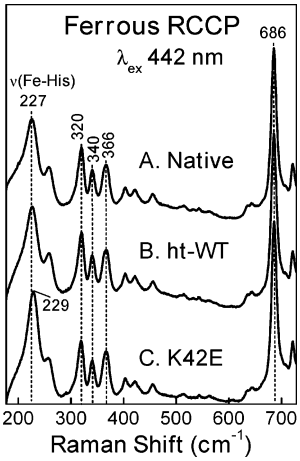

FIGURE 2: Resonance Raman spectra of the ferrous forms of (A) native RCCP; (B) heterologously expressed wild-type RCCP; and (C) RCCP K42E.

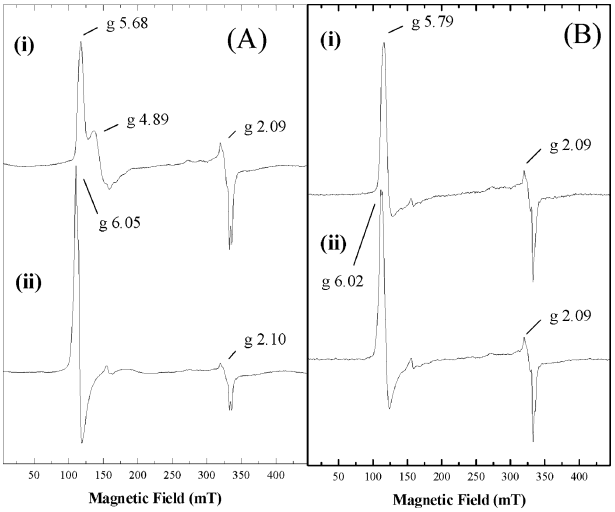

FIGURE 3: EPR spectra of ht-RCCP and RCCP K42E. (A) ht-RCCP at pH 6 (i) and pH 10 (ii). The intermediate spin feature at $g = 4.58$ decreases with incresing pH. (B) RCCP K42E at pH 6 (i) and pH 10 (ii) show only subtle differences. Spectra were collected under the conditions of microwave power 2 mW; microwave frequency 9.39 GHz; modulation amplitude 1.0 mT; temperature 10 K. Five scans were recorded for each species.

intensity, the maximum at 500 nm becomes less pronounced, and the peak at 635 nm increases in intensity from $\epsilon_{635} = 4.3$ to $\epsilon_{635} = 5.7$. At high pH, a distinct shoulder appears around 380 nm. Conversion to the ferrous state by reduction with dithionite ablates the 635-nm feature, causes the Soret band to shift to 430 nm, and results in a broad peak in the α/β region centered at 550 nm. The similarity between the RR spectra of ferrous of ht-WT and native RCCP provides additional evidence that both proteins are identical (Figure 2). In particular, it can be seen that ht-RCCP and native RCCP both exhibit their ν(Fe−His) frequency at 227 cm^{-1}, implying that they have identical Fe−His bond strengths.

The K42E Mutation Does Not Affect the Oligomerization State or Secondary Structure of RCCP. The RCCP used in the present study is identical in sequence to that found in strain MT1131, which has been previously shown to be predominantly monomeric in solution. This behavior contrasts with RCCP isolated from M110 strains that have been shown to exist as monomer/dimer mixtures in solution (*9*, *13*, *15*−*17*). The difference in oligomerization properties between the two strains is seemingly due to three residue changes (*9*, *13*). However, the key electrostatic interaction at the dimer interface between Glu39 and Lys42 is still possible in both strains (*16*). In the present study, AUC indicates that both ht-RCCP and the K42E mutant are monomeric in solution, with no evidence for a monomer/dimer mixture (Figure S1, Supporting Information). The AUC measurements were conducted using protein concentrations (1.5−50 μM) similar to those used for the spectroscopic experiments within this study. Far-UV CD measurements (Figure S2, Supporting Information) also reveal that there is no observable difference in the secondary structure in ht-RCCP and RCCP K42E.

The K42E Mutation Alters the Ferric Spin-State Equilibrium. Ferric cytochromes *c*′ are characterized by a pH-dependent spin-state equilibrium between a quantum-mechanically admixed high-spin/intermediate-spin state (QS) present at low pH and a pure high-spin (HS) state at high pH. Reported pK_a values for this transition range between ~7 and 10, depending on the type of cytochrome *c*′. In the case of RCCP, the pK_a is reported to be 8.4 (*18*). The nature of the spin state in ferric cytochrome *c*′ can be revealed by spectroscopic measurements including UV−vis absorption, RR, and EPR. In the case of ferric ht-RCCP, the QS species present at pH 6 is associated with a Soret absorption maximum at 399 nm, whereas the HS species present at pH 10 has a Soret maximum at 404 nm and a pronounced shoulder near 380 nm (Figure 1). By contrast, there is no significant change in the UV−vis spectrum of ferric K42E over the pH range 6−10 (Figure S3, Supporting Information). Instead, the UV−vis spectrum of ferric K42E is similar to that of the low pH-form of ht-RCCP, implying that K42E remains in the QS and that the pK_a for conversion to the pure HS state is >10.

The ferric spin-state properties of ht-RCCP and the RCCP K42E mutant were also compared using EPR spectroscopy on frozen samples maintained at 10 K. Figure 3A shows the EPR spectra of wild-type Fe(III) RCCP at pH 6 and pH 10. With increasing pH the feature at $g = 4.89$, which is due to QS iron disappears, and the intensity of the HS spin feature at $g = 6.05$ increases. The pH-dependent EPR properties of ht-RCCP are similar to those previously reported for native RCCP (*18*). EPR spectra of K42E reveal no evidence of a QS species between pH 6 and 10 (Figure 3B). Instead, the EPR spectra contain only a HS feature at $g = 5.97$, with the only influence of pH being a subtle change in the HS signal at pH 10. The EPR assignment of K42E as a pure HS species contrasts starkly with the UV−vis data that indicate that K42E is present largely in the QS state. The reason for this discrepancy most likely stems from the fact that that the EPR spectra were obtained at 10 K, whereas the absorption data are from samples at room temperature. It is possible that the RCCP K42E is locked in a stable QS form at room temperature but a stable HS form at 10 K, whereas the spin-state equilibrium of native and ht-RCCP does not appear to be as temperature sensitive, since the EPR data at 10 K and the visible spectroscopies at room temperature clearly show the conversion from the QS to the HS form between pH 6 and 10.

RR measurements provide another means of characterizing the spin state of ferric cytochromes *c*′ via their porphyrin

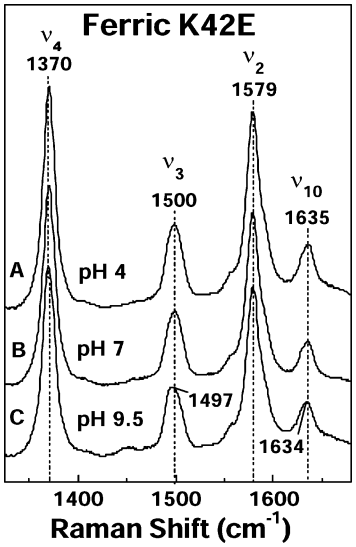

FIGURE 4: Resonance Raman spectra of ferric RCCP K42E at (A) 4.0, (B) pH 7.0, and (C) pH 9.5.

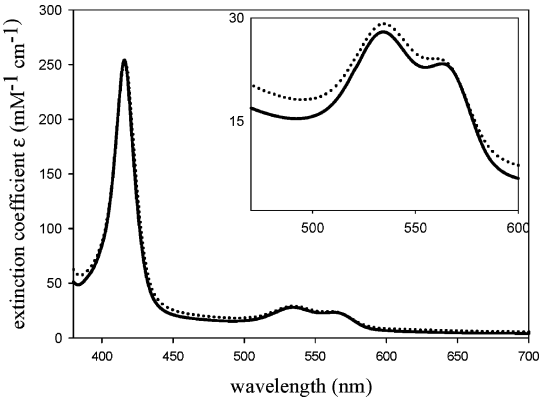

FIGURE 5: UV−vis absorption spectra of the CO complexes of ferrous ht-RCCP (solid line) and RCCP K42E (dotted line). Spectral peaks are centered at 416, 534, and 563 nm.

spin-state marker bands. A recent RR study by our group found that native RCCP at pH < 7 exhibits broad ν_3 and ν_{10} bands containing superpositions of the QS ($\nu_3 = 1502$ cm^{-1}, $\nu_{10} = 1637$ cm^{-1}) and HS components ($\nu_3 = 1494$ cm^{-1}, $\nu_{10} = 1630$ cm^{-1}). This same study showed that upon increasing the pH to 9.5 (beyond the spin-state pK_a of 8.4), the ν_3 and ν_{10} vibrations of native RCCP sharpened to reveal only the HS component (*29*). In the present study, RR spectra of ferric K42E were obtained on samples within the pH range 4−9.5 (Figure 4). At pH 4 and pH 7, K42E exhibits broad ν_3 and ν_{10} bands centered at ∼1500 and ∼1635 cm^{-1}, implying the presence of both QS and HS forms. Upon raising the pH to 9.5 the apparent frequencies of the ν_3 and ν_{10} bands downshift slightly to ∼1496 and ∼1634 cm^{-1}, respectively, consistent with a minor increase in the HS population relative to the QS species. Nevertheless, it is clear that even at pH 9.5, there is still a significant proportion of QS species present in ferric K42E. Taken together, our RR and UV−vis absorption data indicate that ferric K42E at room temperature consists of an equilibrium mixture QS and HS iron that is relatively insensitive to pH within the range 4−9. The fact that the RR data for K42E only show a very small increase in the proportion of the HS species at pH 9.5 suggests that K42E has a spin-state pK_a > 9.5, in contrast to the pK_a of 8.4 for wild-type protein.

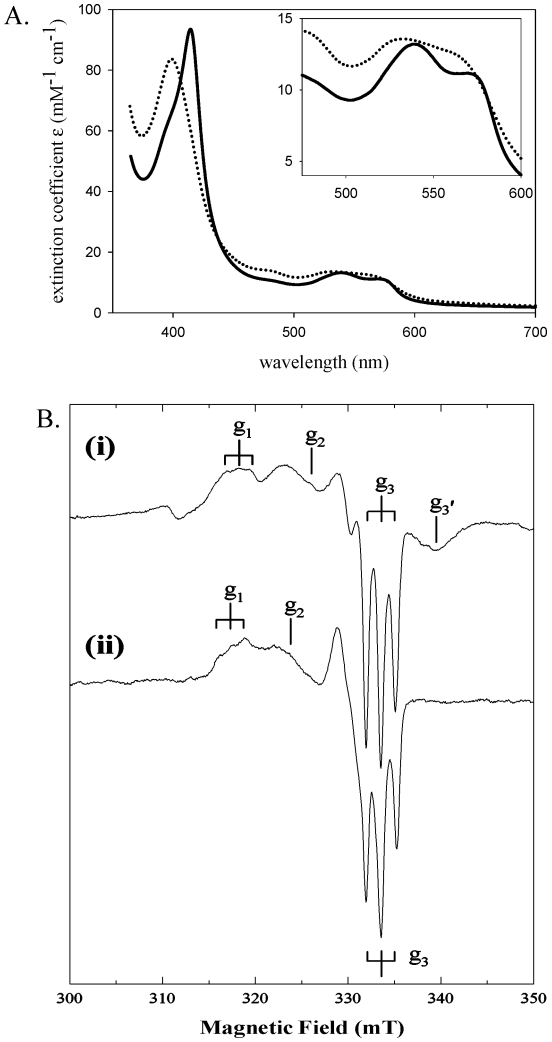

FIGURE 6: Spectroscopic evidence that the NO complexes of ferrous ht-RCCP and K42E RCCP are different. (A) UV−vis absorption spectra of the NO complexes of ferrous RCCP K42E (dotted line) and ht-RCCP (solid line). The differences are all consistent with a change from mixed five- and six-coordinate Fe(II)−NO in wild-type RCCP to solely five-coordinated Fe(II)−NO in the K42E mutant. ht-RCCP has a Soret band at 414 nm and peaks at 530 and 575 nm, whereas RCCP K42E has a Soret peak at 399 nm and a featureless plateau in the α/β region. (B) EPR spectra of NO complexes of ferrous ht-RCCP and RCCP K42E. The ht-RCCP Fe(II)−NO complex (i) shows the characteristic features of a mixture of five- and six-coordinated Fe(II)−NO heme. The most notable distinguishing feature being the g_3' feature centered at $g = 1.98$. This feature is absent in the spectra of RCCP K42E Fe(II)−NO (ii) which contains only the three line feature typical of a five-coordinate Fe(II)−NO heme. Spectra were recorded with microwave power 5 mW; microwave frequency 9.39 GHz; modulation amplitude 0.3 mT; temperature 77 K. Five scans were recorded for each species.

NO and CO Complexes of Ferrous RCCP. The binding of the uncharged ligands CO and NO to the ferrous forms of ht-RCCP and RCCP K42E was investigated using UV−vis absorption, RR, and EPR spectroscopy. Addition of CO to ht-RCCP and RCCP K42E produces nearly identical UV−vis absorption spectra, implying that both form six-coordinate heme−CO complexes (Figure 5). In contrast, the ferrous forms of ht-RCCP and RCCP K42E react very differently with NO (Figure 6A). ht-RCCP generates a ferrous−nitrosyl species that has a Soret absorption centered at 414 nm with a prominent shoulder at 399 nm, together with peaks in the

Table 1: Summary of Spectral Properties of Wild-Type and RCCP K42E

conditions	spectroscopy	protein	spectral features	interpretation
unligated ferric pH 6, 293 K	UV−vis	wild-type K42E	399 nm Soret 399 nm Soret	K42E mutant remains predominantly in QS state at room temperature even at high pH.
unligated ferric pH 10.5, 293 K	UV−vis	wild-type K42E	404 nm Soret 399 nm Soret	
unligated ferric pH 6, 10 K	EPR	wild-type K42E	*g*-values 5.68, 4.89, 2.09 *g*-values 5.79, 2.09	K42E mutant becomes locked in HS state at low temperature.
unligated ferric pH 10, 10 K	EPR	wild-type K42E	*g*-values 6.05, 2.10 *g*-values 6.02, 2.09	
unligated ferrous pH 7, 293 K	UV−vis	wild-type K42E	430 nm, 550 nm 430 nm, 550 nm	Wild-type and mutant are identical 5-c HS species.
unligated ferrous pH 7, 293 K	RR	wild-type K42E	ν(Fe−His) 227 cm^{-1} ν(Fe−His) 229 cm^{-1}	Marginally stronger Fe−His bond in K42E mutant.
CO-ligated ferrous pH 7, 293 K	UV−vis	wild-type K42E	416, 534, 563 nm 416, 534, 563 nm	No differences between proteins. 6c-CO adduct.
NO-ligated ferric pH 7, 293 K	UV−vis	wild-type K42E	414, 529, 563 nm 414, 529, 563 nm	No differences between proteins. 6c-NO adduct.
NO-ligated ferrous pH 7, 293 K	UV−vis	wild-type K42E	414, 530, 575 nm 399, 480, α/β plateau	Wild-type is mixture of 5c and 6c forms; K42E forms exclusively 5c Fe(II)−NO adduct.
NO-ligated ferrous pH 7, 77 K	EPR	wild-type K42E	g_3' feature at $g = 1.98$ no g_3' feature	

$\alpha\beta$ region at 530 and 575 nm. This absorption spectrum is consistent with a mixture of five- and six-coordinated heme−nitrosyl complexes, in line with that previously reported for native RCCP (*22*). On the other hand, NO binding to ferrous RCCP K42E produces a Soret peak centered at 399 nm with no shoulder, a distinctive peak at 480 nm, and a relatively featureless α/β region. These features are typical of a five-coordinate ferrous−nitrosyl complex, without any significant six-coordinate species present.

EPR spectra of ferrous−nitrosyl ht-RCCP and RCCP K42E both contain a three-line feature due to a five-coordinate heme−NO species (Figure 6B). However, only ht-RCCP (not RCCP K42E) contains a second set of heme−NO features due to a six-coordinate heme−NO species. The g_3' feature has been previously observed in RCCP (*21*), and it is thought to consist of a 9-line spectrum that results from the splitting of the electron spin by two ^{14}N nuclei (from the NO ligand and the His ligand to the heme). This concurs with the electronic spectra, demonstrating that the ferrous−nitrosyl form of ht-RCCP is a mixture of five- and six-coordinated heme−NO, whereas the K42E mutant consists of entirely five-coordinate heme−NO. RR spectroscopy was used to examine the environment occupied by NO in the ferrous−nitrosyl form of RCCP K42E. Previous studies have indicated that the ν(Fe−NO) and ν(N−O) frequencies of five-coordinate ferrous heme−nitrosyl complexes are sensitive to the degree of $Fe^{2+} \rightarrow$ NO backbonding, which in turn can be used to predict the chemical environment of the NO ligand. In this study, RR spectra of ferrous−nitrosyl K42E prepared separately with ^{14}NO and ^{15}NO reveal the ν(Fe−NO) mode at 523 cm^{-1} and the ν(N−O) mode at 1666 cm^{-1} (Figure S4, Supporting Information). This compares to previous RR studies of AXCP in which the ν(Fe−NO) and ν(N−O) modes were identified at 526 and 1660 cm^{-1}, respectively. The unusually low ν(N−O) of AXCP was ascribed to the NO ligand being hydrogen bonded to a positively charged (Arg) residue on the proximal heme face (*20*). The fact that K42E exhibits a lower ν(Fe−NO) and a higher ν(N−O) relative to AXCP is consistent with somewhat weaker backbonding in K42E. One structural interpretation of the RR data is that the NO ligand in K42E is bound proximally, but that the hydrogen bond with the adjacent Arg residue is weaker than that in AXCP, leading to less backbonding. However, the present data does not clearly indicate the location of the NO ligand in K42E since its RR frequencies are midway between those expected for proximally and distally bound NO.

Although ferrous ht-RCCP and RCCP K42E differ significantly in their NO-binding properties, it is notable that both proteins exhibit relatively high ν(Fe−His) frequencies of 227 and 229 cm^{-1}, respectively (Figure 2B,C). The relatively strong Fe−His bonds implied by these frequencies provides further evidence that the coordination number of ferrous heme−nitrosyl species of cytochromes *c*′ is not governed by the strength of the proximal bond (*22*).

NO Binding to Ferric RCCP. Reaction of ferric ht-RCCP with NO at pH 7 yields a six-coordinate ferric heme−nitrosyl complex (Figure S5, Supporting Information). Similarly, NO binds to ferric RCCP K42E to form a six-coordinate ferric heme−nitrosyl complex, as judged by the appearance of UV−vis absorption bands at 414, 529, and 563 nm.

The spectral properties of ht-RCCP and RCCP K42E are summarized in Table 1.

DISCUSSION

The present study describes the establishment of an *E. coli* heterologous overexpression system for RCCP that produces wild-type RCCP that is identical to native RCCP on the basis of UV−vis absorption, EPR, and RR measurements. This system will form the basis for future structure/function studies of cytochrome *c*′ including mechanisms of NO detoxification.

The present study also describes the characterization of the K42E mutant of RCCP and its comparison with wild-type protein. This particular mutation was selected to probe the oligomerization state of RCCP and its effect on heme reactivity. Mutagenesis of Lys42 to Glu should lower the

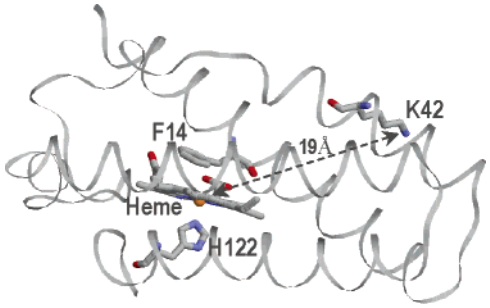

FIGURE 7: Structure model of RCCP indicating location of K42 with respect to the heme. This illustration indicates the large distance between the heme iron of RCCP and the K42 residue (19 Å).

affinity of the monomers for one another since in wild-type a salt bridge occurs between Lys42 and Glu39 on neighboring subunits in the dimer of the crystal structure. Our AUC studies confirm that RCCP K42E is a monomer in solution. However, our AUC studies also reveal that ht-RCCP is monomeric in solution. The oligomerization state of RCCP appears to be sensitive to the experimental conditions, as well as the particular RCCP strain involved. RCCP from *R. capsulatus* MT1131 and related strains has been shown to be an equilibrium mixture of dimer and monomer (predominately monomer) in solution but a dimer in crystal structures (*9*, *8*, *15*, *28*, *30*). The present study indicates that RCCP from our strain is solely monomeric in solution when examined by AUC at the range of concentrations used throughout this investigation.

Although the K42E mutation does not affect the oligomerization state, we found that it does affect some of the properties of the heme center. One major effect is the perturbation of the ferric spin-state equilibrium. At room temperature, the equilibrium is shifted toward the QS form. A variety of structural factors are proposed to favor QS ferric heme centers, including unusually weak axial ligands. Thus, it is possible that the ferric Fe−His bond strength has decreased in the K42E mutant. However, RR spectra of ferrous RCCP K42E and ht-RCCP indicate that in the reduced state, the two proteins have very similar proximal ligand strengths. In terms of ligand binding to the heme center, K42E and wild-type RCCP appear to form similar Fe(III)−NO and Fe(II)−CO complexes. However, spectroscopic evidence shows that the Fe(II)−NO complex in this mutant is five-coordinate, a significant change from RCCP wild-type which forms a mixture of five- and six-coordinate Fe(II)−NO. The fact that RR spectra show similar Fe−His stretching vibrations in the ferrous forms of both K42E and ht-RCCP adds to the emerging picture that the coordination number of ferrous heme−nitrosyl species of cytochromes *c*′ is not dictated by the strength of the Fe^{2+}−His bond.

The finding that mutagenesis of a residue associated with the RCCP dimer interface had an impact on heme chemistry was rather unexpected. Lys42 is distant from the heme (Figure 7), and the mutagenesis does not cause gross changes to the protein secondary structure. However, we must presume that there is some long-range effect of the K42E mutation on the structure of the protein around the heme. Of course, long distance effects of ligand binding or changes in amino acid sequence on the protein structure and properties are well documented in hemoproteins such as hemoglobin and indeed other proteins (see, e.g., ref *31*). The location of residue 42 on helix B, as described in the crystal structure, places it at the dimer interface on the same side of the four helix bundle as the distal vacant sixth coordination site which is RCCP. Residue 42 is surface located and approximately 20 Å from Phe14 which is the hydrophobic residue in the heme pocket that hinders ligand binding in the pocket (*9*, *30*). Another important aspect of the placing of this residue on helix B is its proximity to the deep channel between helix B and C, which has been proposed to be important for ligand access to the distal heme sixth coordination site (*13*). Although an effect close to the Lys42 residue itself might affect access to the deep channel that is proposed to allow ligand access to the distal coordination site, this cannot explain the changes in spin state in the absence of ligand. The alternatives are a change in the geometry of the heme-coordinating His ligand, subtle changes in other residues around the heme (on either distal or proximal side), or changes to the heme macrocycle conformation. It is intriguing that alteration of a surface residue far away from the heme center can have such an impact on the properties of the environment local to the heme. An exciting possibility is that intermolecular encounters at the protein surface might produce structural changes that could be transmitted to the heme center to modulate the reactivity of cytochrome *c*′ in vivo.

ACKNOWLEDGMENT

The authors thank Dr. Pierre Moënne-Loccoz for assistance with resonance Raman measurements.

SUPPORTING INFORMATION AVAILABLE

Predicted molecular mass of ht-RCCP and RCCP K42E as analyzed by analytical ultracentrifugation (Figure S1); circular dichroism spectroscopy of ht-RCCP and RCCP K42E (Figure S2); UV−vis absorbance spectra of RCCP K42E (Figure S3); effect of isotopic substitution on the low-frequency (Figure S4(i)) and high-frequency (Figure S4(ii)) RR spectrum of the 5c-NO adduct of RCCP K42E; and UV−vis absorption spectra of Fe(III)−NO complexes of ht-RCCP and K42E (Figure S5). This material is available free of charge via the Internet at http://pubs.acs.org.

REFERENCES

1. Cusanovich, M. A., and Gibson, Q. H. (1973) Anomalous ligand binding by a class of high spin *c*-type cytochromes, *J. Biol. Chem. 248*, 822−834.
2. Yoshimura, T., Iwasaki, H., Shidara, S., Suzuki, S., Nakahara, A., and Matsubara, T. (1988) Nitric oxide complex of cytochrome *c*′ in cells of denitrifying bacteria, *J. Biochem. 103*, 1016−1019.
3. Mayburd, A. L., and Kassner, R. (2002) Mechanism and biological role of nitric oxide binding to cytochrome *c*′, *Biochemistry 41*, 11582−11590.
4. Moir, J. W. B. (1999) Cytochrome *c*′ from *Paracoccus denitrificans*: spectroscopic studies consistent with a role for the protein in nitric oxide metabolism, *Biochim. Biophys. Acta. 1430*, 64−72.
5. Cross, R., Aish, J., Paston, S. J., Poole, R. K., and Moir, J. W. B. (2000) Cytochrome *c*′ from *Rhodobacter capsulatus* confers resistance to nitric oxide, *J. Bacteriol. 182*, 1442−1447.
6. Cross, R., Lloyd, D., Poole, R. K., and Moir, J. W. B. (2001) Enzymatic removal of nitric oxide catalyzed by cytochrome *c*′ in *Rhodobacter capsulatus*, *J. Bacteriol. 183*, 3050−3054.
7. Anjum, A. F., Stevanin, T. M., Read, R. C., and Moir, J. W. B. (2002) Nitric oxide metabolism in *Neisseria meningitidis*, *J. Bacteriol. 184*, 2987−2993.

8. Shibata, N., Iba, S., Misake, S., Meyer, T. E., Bartsch, R. G., Cusanovich, M. A., Morimoto, Y., Higuchi, Y., and Yasuoka, N. (1998) Basis for monomer stabilization in *Rhodopseudomonas palustris* cytochrome *c*′ derived from the crystal structure, *J. Mol. Biol. 284*, 751−760.
9. Tahirov, T. H., Misaki, S., Meyer, T. E., Cusanovich, M., Higuchi, Y., and Yasuoka, N. (1997) Structure of cytochrome *c*′ from *Rhodobacter capsulatus* strain St Louis: an unusual molecular association induced by bridging Zn ions, *Acta Crystallogr. D. Biol. Chrystallogr. 53*, 658−664.
10. Ren, Z., Meyer, T., and McRee, D. E. (1993) Atomic structure of a cytochrome *c*′ with an unusual ligand-controlled dimer dissociation at 1.8 Å resolution, *J. Mol. Biol. 234*, 433−445.
11. Finzel, B. C., Weber, P. C., Hardman, K. D., and Salemme, F., R. (1985) Structure of ferricytochrome *c*′ from *Rhodospirillum molischianum* at 1.67 Å resolution, *J. Mol. Biol. 186*, 627−643.
12. Yasui, M., Harada, S., Kai, Y., Kasai, N., Kusunoki, M., and Matsuura, Y. (1992) Three-dimensional structure of ferricytochrome *c*′ from *Rhodospirillum rubrum* at 2.8 Å resolution, *J. Biochem. 111*, 317−324.
13. Tahirov, T. H., Misaki, S., Meyer, T. E., Cusanovich, M. A., Higuchi, Y., and Yasuoka, N. (1996) High-resolution crystal structures of two polymorphs of cytochrome *c*′ from the purple phototrophic bacterium *Rhodobacter capsulatus*, *J. Mol. Biol. 259*, 467−479.
14. Dobbs, A. J., Anderson, B. F., Faber, R. H., Faber, and Baker, E. N. (1996) Three-dimensional structure of cytochrome *c*′ from two *Alcaligenes* species and the implications for four-helix bundle structures, *Acta Crystallogr. D 52*, 356−368.
15. Cusanovich, M. A. (1971) Molecular weights of some cytochrome *c*′ *Biochim. Biophys. Acta 236*, 238−241.
16. Tsan, P., Hus, J. C., Caffrey, M., Marion, D., and Blackledge, M. (2000) Rotational diffusion anisotrophy and local backbone dynamics of carbon monoxide-bound *Rhodobacter capsulatus* cytochrome *c*′, *J. Am. Chem. Soc. 122*, 5603−5612.
17. Tahirov, T. H., Misaki, S., Meyer, T. E., Cusanovich, M. A., Higuchi, Y., and Yasuoka, N. (1996) Concerted movement of side chains in the heme vicinity observed on ligand binding in cytochrome *c*′ from *Rhodobacter capsulatus*, *Nat. Struct. Biol. 3*, 459−464.
18. Monkara, F., Bingham, S., J., Kadir, F. H. A., McEwan, A. G., Thomson, A. J., Thurgood, A. G. P., and Moore, G. P. (1992) Spectroscopic studies of *Rhodobacter capsulatus* cytochrome *c*′ in the isolated state and in intact cells, *Biochim. Biophys. Acta 1100*, 184−1088.
19. Fujii, S., Yoshimura, T., Kamada, H., Yamaguchi, K., Suzuki, S., Shidara, S., and Takakuwa, S. (1995) Electron paramagnetic resonance studies of ferric cytochrome *c*′ from photosynthetic bacteria, *Biochim. Biophys. Acta 1251*, 161−169.
20. Andrew, C. R., Green, E. L., Lawson, E. L., and Eady, R. R. (2001) Resonance Raman studies of cytochrome *c*′ support for the binding of NO and CO to opposite sides of the heme: implications for ligand discrimination in heme-based sensors, *Biochemistry 40*, 4115−4122.
21. Yoshimura, T., Fujii, S., Kamada, S., Yamaguchi, K., Suzuki, S., Shidara, S., and Takakuwa, S. (1996) Spectroscopic characterization of nitrosylheme in nitric oxide complexes of ferric and ferrous cytochrome *c*′ from photosynthetic bacteria, *Biochim. Biophys. Acta 1292*, 39−46.
22. Andrew, C. R, Kemper, L. J., Busche, T. L., Tiwari, A. M., Kecskes, M. C., Stafford, J. M., Croft., L. C., Lu, Shen., Moenne-Loccoz, P., Huston, W. M., Moir, J. W. B., and Eady, R. R. (2005) Accessibility of the distal heme face, rather than Fe−His bond strength determines the heme-nitrosyl coordination number of cytochromes *c*′: evidence from spectroscopic studies, *Biochemistry 44*, 8664−8672.
23. Doyle, M. L., Gill, S. J., Cusanovich, M., A. (1986) Ligand-controlled dissociation of *Chromatium vinosum* cytochrome *c*′, *Biochemistry 25*, 2509−2516.
24. Turner, S., Reid, E., Smith, H., and Cole, J. (2003) Mutational and biochemical analysis of cytochrome *c*′, a nitric oxide-binding lipoprotein important for adaptation of *Neisseria gonorrhoeae* to oxygen-limited growth, *Biochem. J. 373*, 865−873.
25. Laemmli, U. K. (1970) Cleavage of structural proteins during the assembly of the head of bacteriophage T4, *Nature 227*, 680−685.
26. Goodhew, C. F., Brown, K. R., and Pettigrew, G. W. (1986) Heme staining in gels, a useful tool in the study of bacterial *c*-type cytochromes, *Biochim. Biophys. Acta 852*, 288−294.
27. Furhop, J. H. (1975) *Laboratory Methods in Porphyrin and Metalloporphyrin Research*; Elsevier Scientific Publishers, New York.
28. Caffrey, M., Simorre. J. P, Cusanovich, M., and Marion, D. (1995) Characterization of the dynamic properties of *Rhodobacter capsulatus* ferricytochrome *c*′ - a 28 kDa paramagnetic heme protein, *FEBS Lett. 368*, 519−522.
29. Servid, A. E., McKay, A. L., Tiwari, A. M., Kecskes, M. C., Stafford, J. M., Moenne-Loccoz, P., Huston, W. M., Moir, J. W. B., Eady, R. R., and Andrew, C., manuscript in preparation.
30. Demene, H., Tsan, P., Gans, P., and Marion, D. (2000) NMR determination of the magnetic susceptibility anisotrophy of cytochrome *c*′ of *Rhodobacter capsulatus* by 1JHN dipolar coupling constants measurement: characterization of its monomeric state in solution, *J. Phys. Chem. B 104*, 2559−2569.
31. Gunasekaran, K., Ma, B., and Nussinov, R. (2004) Is allostery an intrinsic property of all dynamic proteins? *Proteins, 57*, 433−443.

BI052605J